Synthesis of Pt nanoparticles anchored on graphene-encapsulated Fe_3O_4 magnetic nanospheres and their use as catalysts for methanol oxidation

Shaoxiong Lin [a,b], Chengmin Shen [b], Daban Lu [a], Chunming Wang [a,*], Hong-Jun Gao [b]

[a] College of Chemistry and Engineering, Lanzhou University, Lanzhou 730000, China
[b] Beijing National Laboratory of Condensed Matter Physics, Institute of Physics, Chinese Academy of Sciences, Beijing 100190, China

ARTICLE INFO

ABSTRACT

Reduced graphene oxide (rGO)-encapsulated amine functionalized Fe_3O_4 magnetic nanospheres (AMs), were used to support Pt catalysts (Pt-rGO-AMs). The Pt-rGO-AMs were fabricated by modifying positively-charged aminopropyltrimethoxysilane on the surface of Fe_3O_4 nanoparticles (NPs) to form functionalized Fe_3O_4 NPs. Then negatively-charged graphene oxide (GO) was coated on the surface of the functionalized Fe_3O_4 nanospheres by electrostatic layer-by-layer self-assembly. Finally, Pt NPs were uniformly anchored on the surface of GO by a polyol reduction reaction and the GO was simultaneously reduced to rGO. The Pt-rGO-AMs exhibit excellent ferromagnetic property, which makes it possible to realize controllable on–off reactions and convenient recycling of catalyst materials. The electrochemical activity of the catalyst for methanol oxidation is significantly improved compared to Pt NPs absorbed on a rGO sheet and has better stability. The superior performance of this Pt-rGO-AMs catalyst is attributed both to the structure, which improve the accessibility of the Pt NPs by exposing them on the surface of the support, and to the greatly improved electronic conductivity of the support.

1. Introduction

Pt nanoparticles (NPs) have attracted much attention for their superior catalysis for many chemical reactions [1–3], especially for hydrogen oxidation and oxygen reduction in fuel cell reactions [4]. However, high surface energy of NPs with diameters in nanometers often leads to aggregation and catalytic activity decreasing [5]. In order to improve catalytic activity, carbonaceous materials, such as mesoporous carbon [6], graphite [7] and CNTs [8], have generally been employed as the support materials for Pt NPs in fuel cells. Since these supports have relatively low surface areas to accommodate highly concentrated Pt NPs catalysts, graphene with one atom thick planar sheet of hexagonally arrayed sp^2 carbon atoms has been synthesized as an alternative [9]. Graphene exhibits excellent electrical conductivity and extremely high specific surface area ($2620 \, m^2 \, g^{-1}$), which could be explored as a support material to improve both the electro-catalytic activity and stability of Pt NPs for fuel cell reactions [10].

However, it is difficult for an electrolyte to penetrate into the basal layers when graphene nanosheets are used as modified electrode material in electrocatalytic process. When catalysts are dropped on the electrode, Pt NPs may be covered by the stack of the layered graphene sheets, which preventing some Pt NPs from being exposed on the surface of the electrode (see Fig. 1a for a schematic of Pt-graphene). That means Pt NPs will not be fully utilized. Therefore, to have the graphene layers in a structure of zero-dimensional (0D) nanospheres is expected to improve the exposure area of graphene layers as support materials for Pt NPs (Fig. 1b).
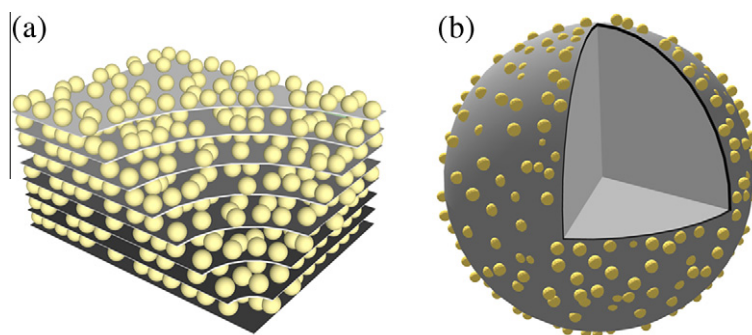
Fig. 1 – Schematic of the (a) Pt-rGO and (b) Pt-rGO-AMs.

In this paper, we report on a novel Pt NPs support material, reduced graphene oxide (rGO)-encapsulated amine functionalized Fe_3O_4 magnetic nanospheres (AMs) (rGO-AMs), to improve the utilization of Pt NPs for methanol electrooxidation. As a catalyst support, the Fe_3O_4 magnetic spheres make it possible to realize controllable on–off reactions and convenient recycling of catalyst materials [11–13]. As another catalyst support material, rGO is expected to improve the catalyst's electro-catalytic activity and stability [14–16]. Moreover, to the best of our knowledge, Pt NPs anchored directly on the surface of Fe_3O_4 are very difficult to obtain. It requires an intermediary, such as silica [17]. It is known that silica is not a good conductor. However, it is expected that the hybrid prepared in our work would present better performance in the methanol oxidation reaction (MOR). Thus, a new intermediary was needed, which can improve the transfer of charge. Graphene used here has excellent electronic conductivity, and could be explored as a support material to improve both the electro-catalytic activity and stability of Pt NPs for fuel cell reactions. Moreover, graphene oxide (GO) is the original basic material for the preparation of individual graphene sheets with abundant oxygen-containing surface functionalities, such as hydroxyl, carbonyl, carboxyl and epoxide groups. These groups allow GO sheets to have a high water solubility and offer potential use as a supporting material for dispersing noble metal NPs to form flexible GO-based hybrid materials. Combined as a support material, Fe_3O_4 nanospheres and graphene oxide (GO) can improve the accessibility of Pt NPs as much as possible by exposing them on the surface of the support. This support material was initially fabricated via combining Fe_3O_4 nanospheres and GO by a simple electrostatic assembly. Then, catalyst NPs were anchored on the surface of GO by a reduction reaction and the GO was simultaneously reduced into rGO. We evaluated the resulting structure's electrochemical behavior, and the electrocatalytic activity of Pt NPs anchored on rGO-AMs for methanol oxidation are significantly improved compared to them absorbed on rGO sheets and have better stability.

2. Experimental

2.1. Materials

Graphite power and Ferric chloride ($FeCl_3 \cdot 6H_2O$) were obtained from Sigma. Chloroplatinic acid (H_2PtCl_6) was from Tianjin

Chemical Factory (Tianjin, China). Polyethylene glycol (PEG, 800 kW) was supplied by Tianjin Guangfu Chemical Reagent Co., Ltd. (China). Aminopropyltrimethoxysilane (APTMS) and tetraethoxysilane (TEOS) were purchased from Acros Organics (New Jersey, USA). Other chemical reagents were of analytical grade and used without further purification.

2.2. Synthesis of $Fe_3O_4@SiO_2@NH_2$ (AMs)

First, the Fe_3O_4 nanospheres were prepared as described in previous reports [18,19]. Briefly, $FeCl_3 \cdot 6H_2O$ (1.35 g), PEG (1.0 g) and sodium acetate (3.6 g) were dissolved in ethylene glycol (EG, 40 mL) under magnetic stirring. The homogeneous yellow solution so obtained was transferred to a Teflon-lined stainless-steel autoclave. Then it was heated to 200 °C and kept at that temperature for 8 h. After that, the autoclave was cooled to room temperature. The black magnetite particles so obtained were washed with ethanol and purified by a magnet for several times and then dried in vacuum at 60 °C for 12 h. Subsequently, the Fe_3O_4 obtained (0.4 g) was dispersed in 10 mL of deionized water, then mixing with 1.0 mL of aqueous ammonia solution (25 wt.%) and 100 mL of ethanol. Next, 1.0 mL of TEOS was added dropwise into the solution under vigorous stirring at room temperature. The stirring continued at room temperature for 24 h to obtain the $Fe_3O_4@SiO_2$ [20]. Finally, the above composites were chemically modified by using APTMS. Typically, $Fe_3O_4@SiO_2$ (0.5 g) and APTMS (1.0 mL) were dissolved in toluene to give a mixture solution (50 mL). The mixture was refluxed for 12 h under nitrogen. The resultant particles were separated with the help of a magnet and then washed with ethanol. Then the product was dried in vacuum at 60 °C for 24 h to obtain the amine functionalized Fe_3O_4 particles (AMs).

2.3. Preparation of GO-AMs and Pt-rGO-AMs

GO was synthesized from natural graphite powder by a modified Hummers method [21,22]. In order to study the component of the synthesized GO. A base wash of GO was investigated using Rourke's method [23]. The experiment is described in the Supplementary material. The base-washed GO and oxidized debris were found to be respectively about 65% and 32% of the GO content, (note that their masses were measured independently, but within experimental error mass balance was still achieved from these two components alone).

These results were similar to those of Rourke. GO-AMs were prepared in an EG-water system (Fig. 2a). In brief, 9.0 mg GO and 45.0 mg AMs were added into 75 mL aqueous solution. And then the mixture was ultrasonically treated for 1.5 h to form a stable colloid. Next, 75 mL of EG was injected into the mixture at room temperature for 1 h under vigorous stirring. Pt-rGO-AMs were synthesized by adding 0.01 mM H_2-$PtCl_6$ to the mixture and then the mixture was kept at 120 °C for 24 h under vigorous stirring (Fig. 2b). The products were finally separated via filtration and washed with deionized water with the help of a magnet several times, then dried under vacuum at room temperature.

2.4.   Characterization

Fourier transform Infrared spectra (FTIR) were recorded with a model 360 Nicolet AVATAR FT-IR spectrophotometer. Raman spectrum was carried out using an in via Raman microprobe (Renishaw Instruments, England) with 514 nm laser excitation. X-ray diffraction (XRD) analysis was performed on a Bruker D8-ADVANCE diffractometer (Cu Kα 1.5406 Å). The chemical composition of the sample was analyzed by X-ray photoelectron spectroscopy (XPS, ESCA LAB 210 Mg Kα). The magnetic properties were measured using a vibrating sample magnetometer (VSM, Lake Shore, USA) by measuring the applied field dependence of magnetization between −20, 000 and 20, 000 Oe at 300 K. The analysis of the composition of the catalyst was obtained with a Thermo IRIS Intrepid II inductively coupled plasma atom emission spectrometry (ICP-AES) system. Field-emission scanning electron microscope (FE-SEM) (XL-SFEG, FEI Corp.), Transmission electron microscopy (TEM) (HITACHI H-8100) and high-resolution transmission electron microscopy (HRTEM) (Tecnai F20, FEI Corp.) were employed to characterize the morphology and crystalline structure of particles.

2.5.   Electrochemical measurement

All electrochemical measurements were carried out with CHI 660d electrochemical workstation, using a three-electrode test cell. A conventional three-electrode system was used with a modified glassy carbon (GC) electrode (5 mm in diameter) was used as the working electrode, on which 20 μL of a paste of the catalyst was applied. The paste was a 0.05 wt.% with the catalyst's concentration approximately 4 mg mL^{-1}. A Pt wire was used as the counter electrode and a saturated calomel electrode (SCE) was used as the reference electrode. Before electrochemical measurements, the solutions were de-aired by blowing purified N_2 (30 min). All measurements were conducted at ambient conditions.

3.   Results and discussion

3.1.   Characterization of Pt-rGO-AMs

Sphere-shaped Fe_3O_4 particles were synthesized as a supporting material for a thin layer of SiO_2 in order to promote electrostatic interactions with the graphene sheets after amidation. The amine modified surface introduces a positive charge, a few layers of GO with negative charge can be loaded on the surfaces of the AMs. Finally, Pt NPs were anchored on the surface of the GO via reduction reaction and the GO was also simultaneously reduced to rGO. In this process, GO is the original basic material for the preparation of individual graphene sheets with abundant oxygen-containing surface functionalities, such as hydroxyl, carbonyl, carboxyl and epoxide groups. These groups make GO sheets negatively-charged. So, it can encapsulate the AMs (positively-charged) by electrostatic layer-by-layer self-assembly. Furthermore, the functional groups can be used as anchoring sites for Pt NPs. That means GO plays an important role in the synthesis of hybrid. The morphology changes in the synthesis process of Pt-rGO-AMs are shown in Fig. 3. It can be seen clearly from the SEM image (Fig. 3a) that the size of the Fe_3O_4 particles is uniform and they have smooth surfaces. The diameter of the Fe_3O_4 particles is 380 ± 5 nm. The morphology of the particles does not change when an SiO_2 layer is coated on the surface of Fe_3O_4 particles to form core–shell $Fe_3O_4@SiO_2$ particles (Fig. 3b). The reason comes from a fact that the thickness of SiO_2 layer is thinner. The SEM image of the particles after being modified by APTMS molecules was shown in the Fig. 3c. It can be observed that the surface of particle remains smooth and there is no change in the diameter of particles. Due to the amine radical, the surfaces of particles are positively charged. The AMs are easily coated by negatively charged GO through electrostatic interactions [24–26]. From Fig. 3d, it is found that the surfaces of the AMs gradually become slight rough, indicating GO is coated on the surface. In this step, the particles are still spherical and have a narrow size distribution (390 ± 10 nm). The monodispersive Pt NPs were then successfully synthesized and anchored on the surface of GO-AMs using polyol method. The SEM image of composites is shown in Fig. 3e. It is seen clearly that the morphology of particles differs from GO-AMs. The change in the morphology of the particles may derive from Pt NPs uniformly distributed on the surface of the particles.
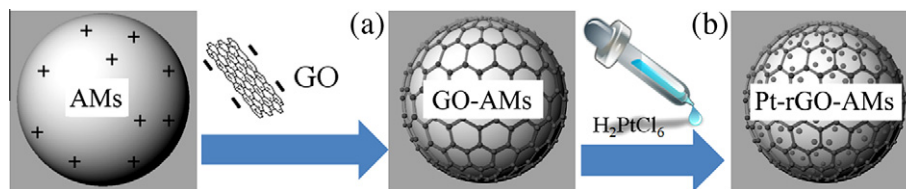

Fig. 2 – Schematic illustration of synthesis step for Pt-rGO-AMs hybrid. (a) Synthesis step of GO-AMs. The hybrid was synthesized through electrostatic interactions. (b) Synthesis step of Pt-rGO-AMs. The hybrid was synthesized through one-step co-reduction of GO and H_2PtCl_6.
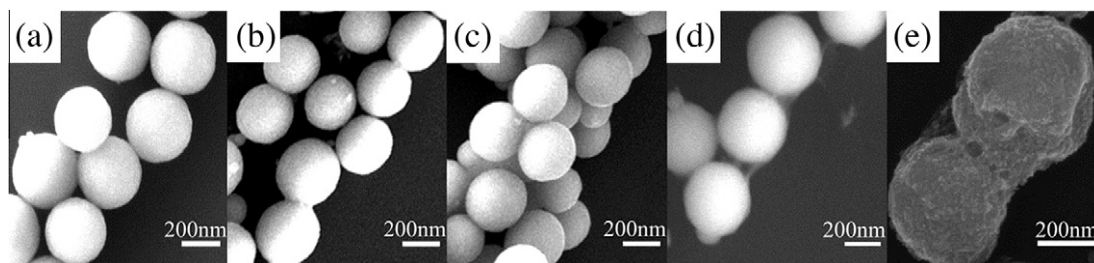
Fig. 3 – Scanning electron microscopy (SEM) images of (a) Fe₃O₄ particles, (b) Fe₃O₄@SiO₂ microspheres, (c) AMs, (d) GO-AMs and (e) Pt-rGO-AMs.

The detailed morphology and structure of composite particles in different strategies were further studied by TEM and results were shown in Fig. 4. The as-synthesized Fe₃O₄ spheres showed in Fig. 4a have good dispersity and have a mean diameter of 380 nm, which is consistent with the re-
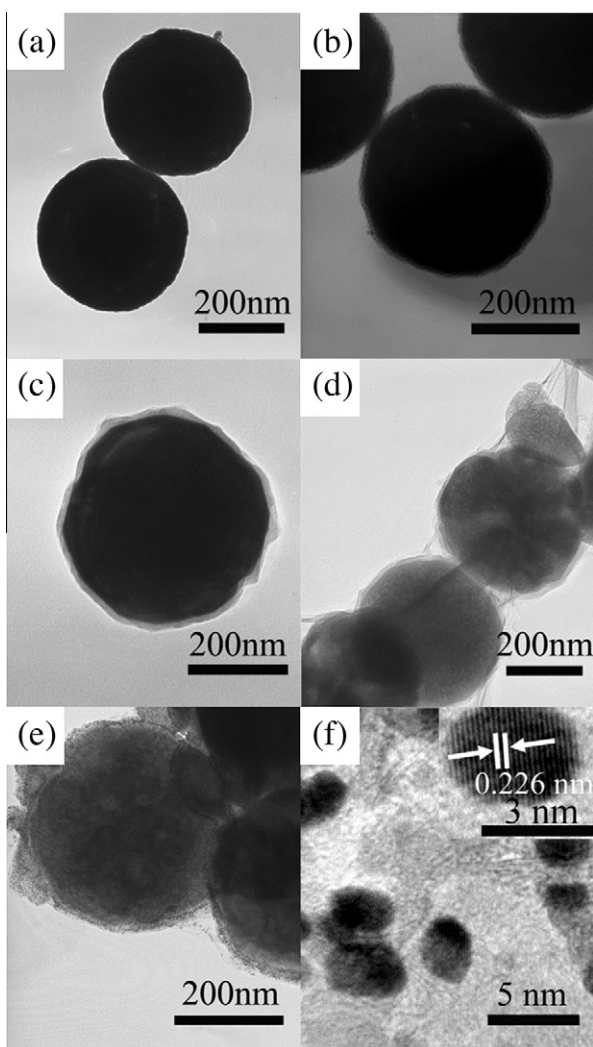

Fig. 4 – Transmission electron microscopy (TEM) images of (a) Fe₃O₄ particles, (b) Fe₃O₄@SiO₂ microspheres, (c) AMs, (d) GO-AMs, (e) Pt-rGO-AMs and (f) the HRTEM image of Pt NPs loaded on the surface of rGO-AMs: the inset is an HRTEM image of a single Pt NPs.

sults of SEM. Fig. 4b shows that a core/shell structure is formed when SiO₂ layer is coated on the surface of Fe₃O₄ particles. The size of shell is about 8 nm. Similarly, the thickness of shell increases a little after the APTMS molecules are adsorbed on the surface of Fe₃O₄@SiO₂ (Fig. 4c). The thin coating of films can be observed clearly on the surface of particles in the Fig. 4d when GO has been loaded on AMs, as demonstrated from observation in SEM images. From Fig. 4e, we can see that the Pt NPs with diameter of 3.5 nm are uniformly distributed on the surface of the particles. The HRTEM image analysis indicated a lattice fringes with an interfringe distance of approximately 2.26 Å, which is close to the interfringe distance of the (111) planes in the fcc structured Pt (Fig. 4f).

In order to further confirm properties of the surface of composite particles, the molecular structure of the different composites was characterized using FTIR spectra and the results are shown in Fig. 5. The FT-IR spectra of Fe₃O₄ NPs, TEOS and TEOS /APTMS coated Fe₃O₄ NPs are shown in Fig. 5a, respectively. From Fig. 5a, it can be seen that the peaks located at 3420 and 1675 cm^{-1} are assigned to the H–O–H stretching modes and the bending vibration of the free or adsorbed water, respectively. The peak at 2930 cm^{-1} is due to -CH₂– asymmetric and symmetric vibration. Other strong peaks appear in the IR spectrum of Fe₃O₄ NPs. A new peak located at 1102 cm^{-1} is observed after a thin SiO₂ layer coated on the surface of Fe₃O₄ NPs, which is assigned to the vibration of the Si–O bonds. When the functionalization of the surface of Fe₃O₄@-SiO₂ using APTMS molecules through layer-by-layer method, an intense peak appears at 1553 cm^{-1}, indicating that amine radical is modified on the surface of Fe₃O₄@SiO₂ successfully.

The FTIR spectra of Pt-rGO-AMs composites are shown in Fig. 5b. The presence of -OH (v_{O-H} at 3420 cm^{-1}), -CH₂– asymmetric and symmetric vibration (v_{-CH2-} at 2930 cm^{-1}), C=O in carboxylic acid and carbonyl moieties ($v_{C=O}$ at 1740 cm^{-1}), C–OH (v_{C-OH} at 1429 cm^{-1}), C–O–C (v_{C-O-C} at 1220 cm^{-1}) and the superposition of the Si–O (v_{Si-O} at 1102 cm^{-1}) and C–O (v_{C-O} at 1080 cm^{-1}) illustrated that GO is assembled on the surfaces of the AMs NPs. In Pt-rGO-AMs, most peaks of the oxide groups are severely attenuated compared with those of GO-AMs, implying that GO has been reduced to rGO. Moreover, this reduction is further evidenced by a new mode at 1553 cm^{-1}, identified as aromatic C=C [27]. The spectrum of Pt-rGO, as a comparison, also confirms that the GO has been restored.

To illustrate the fabrication of the GO-encapsulated nanospheres and the reduction of GO on the surface, Raman scattering spectra were used to monitor the structural changes of
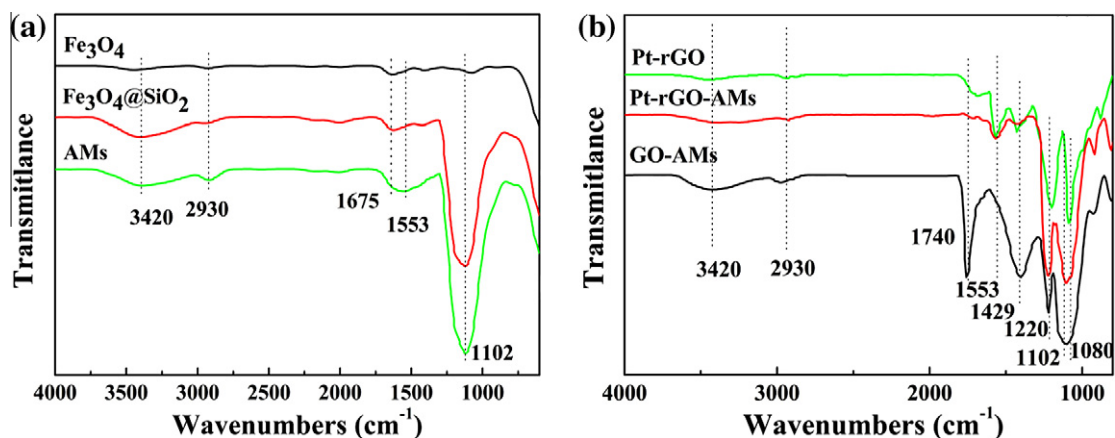
Fig. 5 – FTIR spectra of (a) Fe$_3$O$_4$, Fe$_3$O$_4$@SiO$_2$ and AMs, (b) Pt-AMs, Pt-rGO-AMs and GO-AMs.

carbon materials, and they provide additional evidence of rGO. The Raman spectra for the Pt-rGO-AMs hybrid and GO-AMs are shown in Fig. 6. As Fig. 6a shows, the Raman spectrum of GO-AMs displays a signal at 688 cm^{-1}, corresponding to the Fe$_3$O$_4$ particles. The signal at 1347 cm^{-1} represents the overlap of the Fe$_3$O$_4$ peak and a typical rGO D band peak, and a signal at 1591 cm^{-1} is identified as the G band of rGO [28–30]. After the surface of GO was anchored by Pt NPs, the Raman spectra of Pt-rGO-AMs (Fig. 6b) and Pt-rGO (Fig. S2a) also contained both G and D bands. However, the D/G intensity ratio increased in comparison with GO-AMs, which indicates that the GO has been reduced to rGO and agrees well with earlier reports [22,31].

The crystal structure of composite particles in different strategies was analyzed by XRD. The XRD patterns of a series of Fe$_3$O$_4$ composites including Fe$_3$O$_4$, Fe$_3$O$_4$@SiO$_2$, AMs and Pt-rGO-AMs are presented in Fig. 7. The diffraction peaks located at 18.3°, 30°, 35.4°, 37°, 43°, 53.4°, 57° and 62.6° correspond to the (111), (220), (311), (222), (400), (422), (511) and (440) planes in Fe$_3$O$_4$ cubic lattice, respectively. These results are in good agreement with those XRD patterns of Fe$_3$O$_4$ reported in the literature [18,32], which confirms the cubic spinel structure of the magnetite materials. The specific XRD patterns of Pt-rGO-AMs (Fig. 7d) are characterized by three weak peaks
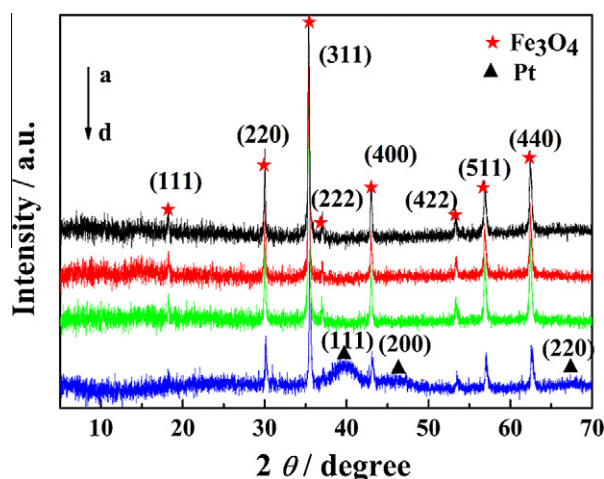

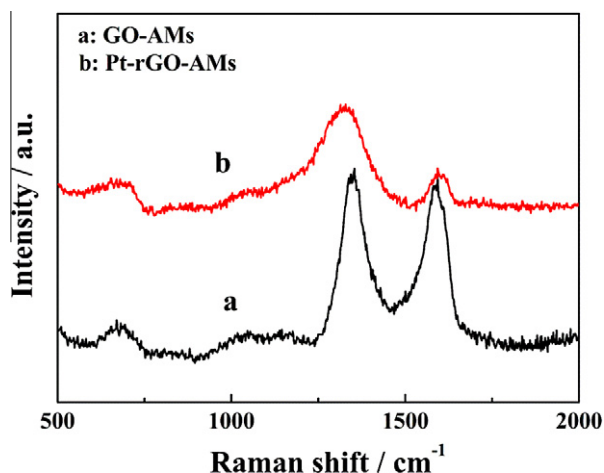Fig. 7 – XRD patterns of (a) Fe$_3$O$_4$, (b) Fe$_3$O$_4$@SiO$_2$, (c) AMs and (d) Pt-rGO-AMs.

positioned at 2θ values of 39.6°, 46.2° and 67.5°, which correspond to the (111), (200) and (220) lattice planes of the face-centered-cubic (fcc) Pt, respectively. This reveals that Pt NPs are successfully anchored on the surface of the nanospheres. According to the Scherrer equation, the average size of Pt NPs, calculated based on Pt (111), is approximately 3.67 nm, which agrees well with the results of TEM investigation. In Fig. 7d, there are no significant diffractions from the rGO, suggesting that the rGO is distributed uniformly to encapsulate the magnetite particles [33]. This is also confirmed by the XPS analysis (Fig. S3).

The magnetic properties of the synthesized Pt-rGO-AMs were investigated using a vibrating sample magnetometer (VSM) at 300 K. The magnetic field *vs.* moment measurements of the solid samples were performed with the magnetic field swept back and forth between +20 and −20 kOe. The saturation magnetic moments obtained are 88.0, 61.8 and 40.9 emu/g for Fe$_3$O$_4$, AMs and Pt-rGO-AMs respectively, as shown in Fig. 8. The coercivity values obtained for the corresponding magnetic materials are ∼42, 60 and 70 Oe (Fig. 8; left top inset). The right bottom inset demonstrates easy manipulation of hybrid microspheres by an external magnetic field
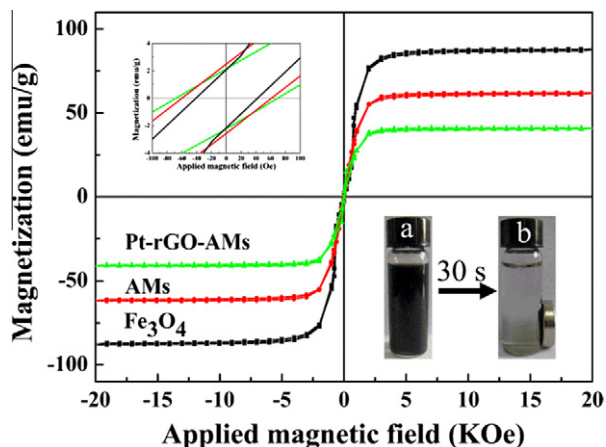

Fig. 6 – Raman spectra of (a) GO-AMs and (b) Pt-rGO-AMs.

Fig. 8 – VSM magnetization curves of Fe₃O₄, AMs and Pt-rGO-AMs at 300 K. The left top inset is the magnified image of VSM; the inset in right bottom is (a) Pt-rGO-AMs dispersion in water; (b) the dispersion of (a) attached to a magnet 30 s later.

(only ~30 s separation can be achieved), which makes it possible to realize controllable on–off reactions and convenient recycling of catalyst.

3.2. Catalytic activities of Pt-rGO-AMs

To evaluate the electro-catalytic activity of the as-prepared catalysts toward methanol oxidation, cyclic voltammetry (CV) was used to estimate the electrochemically active surface area (ECSA) of the catalysts on a GC electrode. According to the ICP-AES results, the contents of Pt in Pt-rGO-AMs and Pt-rGO catalysts are 7.2 and 24.9 wt.%, respectively. The currents of CV tests are normalized to the measured metal loading.

The CV curves for electro-catalyst in 0.5 M H_2SO_4 solution at a scan rate of 50 mV s^{-1} are shown in Fig. 9a. In the potential region of −0.2–0 V (vs. SCE), typical hydrogen desorption peaks from Pt are observed. The integrate area under the desorption peaks in the CV curve (Q_H), has been used to determine ECSA by employing the equation [15,34]

$$ECSA[cm^2/g \text{ of } Pt] = \frac{change[Q_H, C]}{210[\mu C/cm^2] \times \text{electrode loading}[g \text{ of } Pt]}$$

Our calculation indicates that Pt-rGO-AMs have higher ECSA (59.29 m^2 g^{-1}) than Pt-rGO (33.55 m^2 g^{-1}). This result shows the structural advantage of Pt-rGO-AMs can improve the use of Pt NPs on graphene.

The CV curves of the Pt-rGO-AMs and Pt-rGO electrodes in 0.5 M H_2SO_4 containing 1.0 M CH_3OH solution with scan rate of 50 mV s^{-1} are shown in Fig. 9b. Both CV curves show a similar pair of oxidation peaks, which reveals a peak of methanol oxidation in the forward scan and the other one in the backward scan corresponding to the removal of the residual carbonaceous species formed in the forward scan [35]. The higher peak current density is observed on the Pt-rGO-AMs, indicating higher catalytic activity for CH_3OH oxidation, nearly 1.6 times that on Pt-rGO catalyst. This is also consistent with the result of the ECSA. Moreover, the ratio of the forward peak
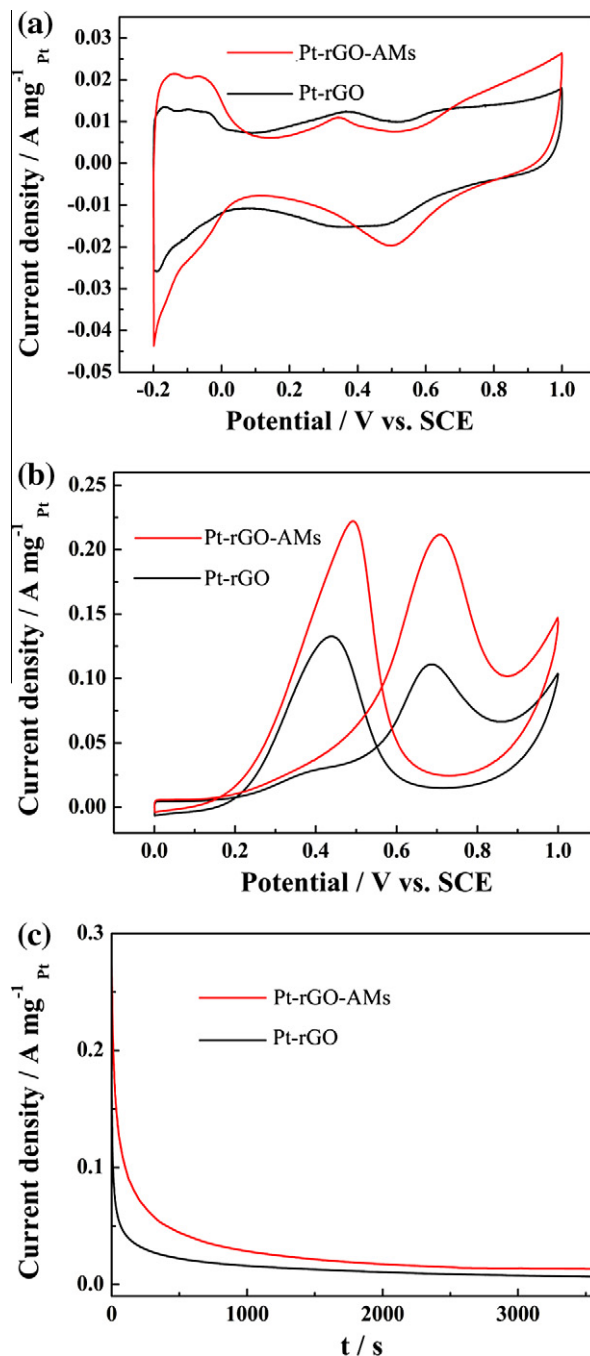

Fig. 9 – Electrochemical catalytic performance Pt-rGO-AMs hybrid and Pt-rGO hybrids. Measurements were performed in (a) 0.5 M H_2SO_4 and (b) 0.5 M H_2SO_4 + 1 M CH_3OH with scan rate of 50 mV s^{-1}. (c) Current–time curves of the hybrids in H_2SO_4 + 1 M CH_3OH at 0.7 V.

current density (I_f) to the back peak current density (I_b), I_f/I_b, can be used to describe the catalyst tolerance to carbonaceous species accumulation [36]. It is interesting to find that the I_f/I_b value is about 0.95 for methanol oxidation on the Pt-rGO-AMs, which is higher than that on Pt-rGO (0.84), indicating that more effective oxidation of methanol occurs on Pt-rGO-AMs during the forward potential scan and that less poisoning species forms compared with Pt-rGO.

The catalytic activity and stability of the hybrid are evaluated by studying its steady-state response with time. The chronoamperometry experiments under 0.7 V in a solution of a 0.5 M H_2SO_4 and 1.0 M CH_3OH are shown in Fig. 9c. Upon the operation, the current gradually reached a quasi-equilibrium steady state. In comparison, the steady-state current on the hybrid is much higher than that on the Pt-rGO. This result is in good agreement with the CV study and implies that the catalytic activity and stability of this hybrid is better than that of Pt-rGO.

Based on the above results, these favorable properties may be attributed to two aspects. First, the AMs serve as a highly conductive support for quickly providing electrons which might be favorable for electrochemical reaction. Second, due to the formation of sphere-shaped rGO-AMs, Pt NPs can be uniformly dispersed over the whole surface. Compared to Pt NPs loaded on the layered graphene, the special structure may improve the accessibility of the Pt NPs. Additionally, the oxidized debris of GO is strongly adhered to the sheets of GO by a combination of π–π stacking and hydrogen bonds in acidic or neutral conditions [23]. Thus, we believe that the oxidized debris will not fall off and affect the catalytic reaction. Since the reaction is done in H_2SO_4 solution in this report.

4. Summary

Graphene-encapsulated functionalized Fe_3O_4 magnetic nanospheres as a novel catalyst-support material were synthesized using an electrostatic layer-by-layer method. The monodispersed Pt NPs were anchored on the surface of the GO-AMs nanospheres by a polyol reduction method and the GO was simultaneously reduced to rGO. The morphology and structure were characterized through SEM, TEM, FT-IR, XRD and Raman spectra. The magnetic properties were investigated by VSM. The study of the electrochemical methanol oxidation showed that Pt-rGO-AMs can improve the catalytic activity over the regular rGO-supported Pt NPs. The excellent performance here indicates that rGO-AMs are a promising catalyst-support material for fuel cell reactions.

Acknowledgements

Appendix A. Supplementary data

Supplementary data associated with this article can be found, in the online version, at http://dx.doi.org/10.1016/j.carbon.2012.10.037.

REFERENCES

[1] Davis RJ, Derouane EG. A non-porous supported platinum catalyst for aromatization of *n*-hexane. Nature 1991;349:313–5.

[2] Bratlie KM, Lee H, Komvopoulos K, Yang P, Somorjai GA. Platinum nanoparticle shape effects on benzene hydrogenation selectivity. Nano Lett 2007;7:3097–101.

[3] An W, Chuang KT, Sanger AR. Catalyst-support interaction in fluorinated carbon-supported Pt catalysts for reaction of NO with NH_3. J Catal 2002;211:308–15.

[4] Steele BCH, Heinzel A. Materials for fuel-cell technologies. Nature 2001;414:345–52.

[5] Zhao M, Sun L, Crooks RM. Preparation of Cu nanoclusters within dendrimer templates. J Am Chem Soc 1998;120:4877–8.

[6] Sua F, Poh CK, Zeng J, Zhong Z, Liu Z, Lin J. Pt nanoparticles supported on mesoporous carbon nanocomposites incorporated with Ni or Co nanoparticles for fuel cells. J Power Sources 2012;205:136–44.

[7] Wang M, Xu F, Sun H, Liu Q, Artyushkova K, Stach EA, et al. Nanoscale graphite-supported Pt catalysts for oxygen reduction reactions in fuel cells. Electrochim Acta 2011;56:2566–73.

[8] He D, Mu S, Pan M. Improved carbon nanotube supported Pt nanocatalysts with lyophilization. Int J Hydrogen Energy 2012;37:4699–703.

[9] Novoselov KS, Geim AK, Morozov SV, Jiang D, Zhang Y, Dubonos SV, et al. Electric field effect in atomically thin carbon films. Science 2004;306:666–9.

[10] Xin Y, Liu J, Liu W, Gao J, Xie Y, Yin Y, et al. Preparation and characterization of Pt supported on graphene with enhanced electrocatalytic activity in fuel cell. J Power Sources 2010;196:1012–8.

[11] Tsang SC, Caps V, Paraskevas I, Chadwick D, Thompsett D. Magnetically separable, carbon-supported nanocatalysts for the manufacture of fine chemicals. Angew Chem Int Ed 2004;43:5645–9.

[12] Lu AH, Li WC, Kiefer A, Schmidt W, Bill E, Fink G, et al. Fabrication of magnetically separable mesostructured silica with an open pore system. J Am Chem Soc 2004;126:8616–7.

[13] Wu S, He Q, Zhou C, Qi X, Huang X, Yin Z, et al. Synthesis of Fe_3O_4 and Pt nanoparticles on reduced graphene oxide and their use as a recyclable catalyst. Nanoscale 2012;4:2478–83.

[14] Nethravathi C, Anumol EA, Rajamathi M, Ravishankar N. Highly dispersed ultrafine Pt and PtRu nanoparticles on graphene: formation mechanism and electrocatalytic activity. Nanoscale 2011;3:569–71.

[15] Li YJ, Gao W, Ci LJ, Wang CM, Ajayan PM. Catalytic performance of Pt nanoparticles on reduced graphene oxide for methanol electro-oxidation. Carbon 2010;48:1124–30.

[16] Shang N, Papakonstantinou P, Wang P, Silva SRP. Platinum integrated graphene for methanol fuel cells. J Phys Chem C 2010;114:15837–41.

[17] Panella B, Vargas A, Baiker A. Magnetically separable Pt catalyst for asymmetric hydrogenation. J Catal 2009;261:88–93.

[18] Deng H, Li X, Peng Q, Wang X, Chen J, Li Y. Monodisperse magnetic single-crystal ferrite microspheres. Angew Chem Int Ed 2005;44:2782–5.

[19] Xuan SH, Wang YJ, Leung KC, Shu KY. Synthesis of Fe_3O_4@polyaniline core/shell microspheres with well-defined blackberry-like morphology. J Phys Chem C 2008;112:18804–9.

[20] Hui C, Shen C, Yang T, Bao L, Tian J, Ding H, et al. Large-scale Fe_3O_4 nanoparticles soluble in water synthesized by a facile method. J Phys Chem C 2008;112:11336–9.

[21] Hummers WS, Offeman RE. Preparation of graphitic oxide. J Am Chem Soc 1958;80:1338–9.

[22] Xu YX, Bai H, Lu GW, Li C, Shi GQ. Flexible graphene films via the filtration of water-soluble noncovalent functionalized graphene sheets. J Am Chem Soc 2008;130:5856–7.

[23] Rourke JP, Pandey PA, Moore JJ, Bates M, Kinloch IA, Young RJ, et al. The real graphene oxide revealed: stripping the

oxidative debris from the graphene-like sheets. Angew Chem Int Ed 2011;50:3173–7.

[24] Myung S, Lee M, Kim GT, Ha JS, Hong S. Large-scale "surface-programmed assembly" of pristine vanadium oxide nanowire-based devices. Adv Mater 2005;17:2361–4.

[25] Lee M, Im J, Lee BY, Myung S, Kang J, Huang L, et al. Linker-free directed assembly of high-performance integrated devices based on nanotubes and nanowires. Nat. Nanotechnol. 2006;1:66–71.

[26] Wang JZ, Zhong C, Wexler D, Idris NH, Wang ZX, Chen LQ, et al. Graphene-encapsulated Fe_3O_4 nanoparticles with 3D laminated structure as superior anode in lithium ion batteries. Chem Eur J 2011;17:661–7.

[27] Zangmeister CD. Preparation and evaluation of graphite oxide reduced at 220 °C. Chem Mater 2010;22:5625–9.

[28] Shebanova ON, Lazor P. Raman study of magnetite (Fe_3O_4): laser-induced thermal effects and oxidation. J Raman Spectrosc 2003;34:845–52.

[29] Cohen H, Gedanken A, Zhong Z. One-Step synthesis and characterization of ultrastable and amorphous Fe_3O_4 colloids capped with cysteine molecules. J Phys Chem C 2008;112:15429–38.

[30] Tang L, Wang Y, Li Y, Feng H, Lu J, Li J. Preparation, structure, and electrochemical properties of reduced graphene sheet films. Adv Funct Mater 2009;19:2782–9.

[31] Zhou K, Zhu Y, Yang X, Luo J, Li C, Luan S. A novel hydrogen peroxide biosensor based on Au-graphene-HRP-chitosan biocomposites. Electrochim Acta 2010;55:3055–60.

[32] Shen J, Zhu Y, Zhou K, Yang X, Li C. Tailored anisotropic magnetic conductive film assembled from graphene-encapsulated multifunctional magnetic composite microspheres. J Mater Chem 2012;22:545–50.

[33] Chen D, Ji G, Ma Y, Lee J, Lu J. Graphene-encapsulated hollow Fe_3O_4 nanoparticle aggregates as a high-performance anode material for lithium ion batteries. ACS Appl Mater Interfaces 2011;3:3078–83.

[34] Girishkumar G, Rettker M, Underhile R, Binz D, Vinodgopal K, Mcginn P, et al. Single-wall carbon nanotube-based proton exchange membrane assembly for hydrogen fuel cells. Langmuir 2005;21:8487–94.

[35] Chang Y, Han G, Li M, Gao F. Graphene-modified carbon fiber mats used to improve the activity and stability of Pt catalyst for methanol electrochemical oxidation. Carbon 2011;49:5158–65.

[36] Yoo E, Okata T, Akita T, Kohyama M, Nakamura J, Honma I. Enhanced electrocatalytic activity of Pt subnanoclusters on graphene nanosheet surface. Nano Lett 2009;9:2255–9.